Synthesis and Characterization of Functionalized Hafnium Oxide Nanoparticles for Supercapacitor Applications

Jayavel M
Presidency College (Autonomous)
Venkatachalam J (venkatmat1980@gmail.com)
Meenakshi College of Engineering https://orcid.org/0000-0002-4014-9905
RAMALAKSHMI N
Presidency College (Autonomous)
SIVASANKARAN A
Yeungnam University

Research Article

Keywords: Hafnium Oxide (HfO2), Sulfonated Hafnium Oxide (S-HfO2), Functionalized Hafnium Oxide, Supercapacitor, Galvanostatic Charge/Discharge and Cyclic Voltammetry

Posted Date: September 7th, 2021

DOI: https://doi.org/10.21203/rs.3.rs-875384/v1

SYNTHESIS AND CHARACTERIZATION OF FUNCTIONALIZED HAFNIUM OXIDE NANOPARTICLES FOR SUPERCAPACITOR APPLICATIONS

M. Jayavel[1,2], N. Ramalakshmi[1,3], J. Venkatachalam[4,*], A. Sivasankaran[5]

[1] Department of Chemistry, Presidency College (Autonomous), Chennai-600 005, India.

[2] Department of Chemistry, Meenakshi College of Engineering, Chennai-600 078, India.

[3] Joint Director, Collegiate Education, Vellore Region, Vellore-632 001, India.

[4] Department of Physics, Meenakshi College of Engineering, Chennai-600 078, India.

[5] Department of Civil Engineering, Yeungnam University, Gyungsan-712 749, South Korea.

*Corresponding author: Name: Dr. J. Venkatachalam, Email: venkatmat1980@gmail.com

Abstract

Functionalized metal oxide electrode material plays an important role in the energy application of the supercapacitor. In this work, the comparative study of super-capacitance performance of hafnium oxide (HfO_2) and sulfonated hafnium oxide (S-HfO_2) nanomaterials is reported. The HfO_2 nanoparticles were synthesized by the precipitation method. Subsequently, the prepared HfO_2 nanoparticles were functionalized using sulfuric acid (H_2SO_4). Further, the synthesized nanoparticles were characterized and confirmed by X-Ray diffraction (XRD), Fourier transform infrared (FT-IR) spectroscopy, High-resolution transmission electron microscope (HR-TEM), Field-Emission scanning electron microscope (FE-SEM) and Energy Dispersive X-Ray spectroscopy (EDS) techniques. The electrochemical properties and ion transfer characteristics of the supercapacitor were investigated by the cyclic voltammeter (CV) and galvanostatic charge-discharge (GCD) experiments. Moreover, the internal resistances of the material (HfO_2 and S-HfO_2) were analysed using Electrochemical Impedance Spectroscopy (EIS) technique. Both the nanoparticles showed a good improvement in specific capacitance.

The supercapacitor values were measured for HfO_2 and S-HfO_2 electrodes which exhibit a specific capacitance value 126 Fg^{-1} and 210 Fg^{-1} respectively at the scan rate 5 mVs^{-1}. Hence, it is noted that functionalized HfO_2 nanoparticle enhances the specific capacitance and is used as a promising material for energy storage device. Moreover, this method is suitable for developing a variety of functionalized metal oxide based nanomaterials for energy applications.

Keywords: Hafnium Oxide (HfO_2), Sulfonated Hafnium Oxide (S-HfO_2), Functionalized Hafnium Oxide, Supercapacitor, Galvanostatic Charge/Discharge and Cyclic Voltammetry**.**

1. Introduction

In recent years, many researchers have shown considerable interest in the development of a supercapacitor using functionalised metal oxide nanoparticles for its high power density, cost effectiveness, long cycle life, safe operation and good ecofriendliness compared to the traditional battery [**1-3**] The traditional charge storage devices like batteries, cannot satisfy the increasing global power demands. In order to overcome the drawbacks of traditional storage devices, scientist and researchers have focused to develop solid state, light weight and flexible supercapacitors, to meet their demands for future. The nature of electrode material plays an important role in the performance of supercapacitor [**4**]. Past few years researchers have cocentrated more on transition metal oxide based supercapacitor due to its pseudocapacitance with fast surface redox reactions, display significantly higher capacitance and energy density [**5**]. So far different transition metal oxides including ruthenium oxide [**6**], manganese oxide [**7**], nickel oxide [**8**], cobalt oxide [**9,10**], iron oxide [**11**] and zirconium oxide [**12**] etc. have been examined for psuedocapacitance capability. Like aforesaid series, hafnium oxide (HfO_2) is also one of the metal oxides in transition metals and it offers a lower cost, less toxic and its availability creates us more interest. Consequently, expectation of nanosized HfO_2 particles towards supercapacitor performance has increased [**13**] and addition of oxides can improve the cycling stability of energy storage devices (ESD) [**14-16**]. But, functionalization and dispersion of metal oxide are of crucial importance for their applications, as they have enormous utilization in several areas including defense, aerospace, electric vehicles and consumer electronics applications [**17**]. This finding gives a clue that nanosized transition metal oxides when functionalise with sulphuric acid could enhance [**18**] the performance of electrochemical electrodes due to their varying oxidation state. However, the roles played by the sulfonated

nanosized HfO_2 particles in the enhancement of super capacitance (SC) have not yet been clearly reported.

In the present study, HfO_2 nanoparticles were successfully synthesised by the precipitation method and further it was functionalized with sulphuric acid to increase the proton conductivity of the nanosized intrinsic HfO_2. Subsequently, both the nanoparticles were characterized. Meanwhile, the electrochemical behaviour of both HfO_2 (before functionalized) and S-HfO_2 (after functionalized) nanoparticles were examined by cyclic voltammeter (CV) and galvanostatic charge-discharge (GCD) techniques followed by internal resistance of (HfO_2 and S-HfO_2) the nanomaterials were measured by Electrical Impedance Spectroscopy (EIS) technique, and afterwards, specific capacitance values of both the nanoparticles were compared.

2. Experimental Details

2.1. Materials

Hafnium tetrachloride ($HfCl_4$, 98%), sodium hydroxide (NaOH. 98%), were purchased from Sigma Aldrich, USA., concentrated sulfuric acid (H_2SO_4), and methanol (CH_3OH) were obtained from Daejug Chemicals & Metals Co., Ltd, Korea and used as received.

2.2. Preparation of HfO_2 Nanoparticles

The HfO_2 nanoparticles were synthesized using a precipitation method [**19**]. Briefly, 0.4 M (100 mL) of NaOH solution was added dropwise to 0.1 M (100 mL) of aqueous $HfCl_4$ solution and stirred for 8 h, resulting in the formation of a hafnium hydroxide (white precipitate). The white precipitate was then washed repeatedly with de-ionized water by centrifugal method at 4000 rpm for 15 min to seperate the residuals. The powder form of final product was dried at 100 °C in a hot air oven for 3 h. Subsequently, it was calcined further at 500 °C for 3 h to obtain HfO_2 nanoparticles.

2.3. Synthesis of Sulfonated-HfO_2 nanoparticles

The prepared HfO_2 nanoparticles (1 g) were mixed in a solution comprised of methanol and sulphuric acid (20 mL of methanol and 15mL of 1 M H_2SO_4) and sonicated it for 2 h. The product was dried at 100°C for 24 h to obtain S-HfO_2 [**20**,**21**]. Then, the dried product of S-HfO_2 was used for further characterization.

2.4. Characterization techniques

The crystal structure, orientation and size of HfO_2 and S-HfO_2 nanoparticles were analyzed by X-ray diffractometer (XRD) (D8 Advance, Bruker, Ettlingen, Germany) using Cu Kα radiation (λ = 1.5406 A°) operated at 40 keV and 30 mA. The presence of functional groups and types of vibrational frequency present in the HfO_2 and S-HfO_2 nanoparticles were confirmed by Fourier Transform Infrared (FT-IR) spectrocopy (Alpha Bruker Spectrometer). The surface morphology of synthesized HfO_2 and S-HfO_2 nanoparticles were examined by HR-TEM (FEI-Tecnai TF-20) and FE-SEM (Model: S-4200, Hitachi, Japan). All the prepared materials were coated with platinum prior to the examination. Elemental analysis was performed using Electron dispersive spectroscopy (EDS) attached to the FE-SEM. The internal resistance of the material was characterized by using Electrical Impedance Spectroscopy (EIS). Before measuring the impedance all the prepared samples (intrinsic HfO_2 and S-HfO_2) were immersed in water at room temperature for 24 h followed by placing the sample between the two electrodes (with 0.62 cm^2 area) with the frequency range of 1-100 Hz and the signal amplitude of 10 mV using an Autolab potentiostat (GSTAT128N, Metrohm Autolab, Utrecht, Netherlands) electrochemical system. The conductivity (σ) was determined using Eq. (1)

$$\sigma = \frac{L}{RA} \tag{1}$$

where σ = proton conductivity of the prepared material (S cm^{-1});

L = thickness of material (cm);

R = material resistance (Ω) and

A = electrode (cm^2) [**22**]

2.5. Electrochemical Measurements

The CV experiments were performed using a Autolab PGSTAT128N, Utrecht, Netherlands to evaluate the electrochemical behavior of the intrinsic HfO_2 and S-HfO_2 under the open-circuit potential. The working electrode was connected to the anode then the connectors of counterelectrode and reference electrode were connected to the cathode. CV was measured in the potential range from 1 to −1 V at scan rates of 10 mVs^{-1}. The configuration and electrode preparation for the study of CV, GCD were explained briefly in results and discussions. The specific capacitance was calculated by integrating the area under the CV curve using equation (2).

$$Cs = \frac{1}{mV\,(V_U - V_L)} \int_{V_L}^{V_U} I(V)dV \qquad (2)$$

where m is the mass of active material (g), V is the scan rate (mVs^{-1}), V_U and V_L are the upper and lower voltage limits (V) and I is the current (A).

In addition to this, the specific capacitance were also calculated from the slope of the galvanostatic charge-discharge curve at the different current densities using the following Eq. (3).

$$C_s = \frac{I\Delta t}{m\Delta V} \qquad (3)$$

where I is the discharge current (mA), m is the mass of the electro-active material (mg) and Δt is the difference in discharge time (t).

3. Results and Discussion

3.1. XRD characterization of HfO_2 and S-HfO_2 nanoparticles.

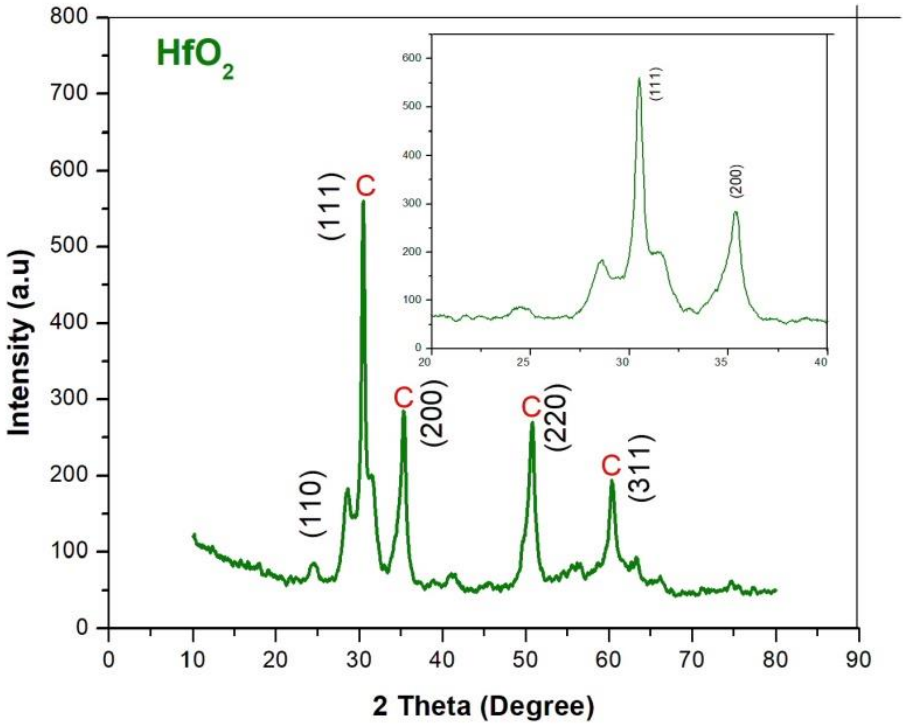

Fig. 1 XRD pattern HfO_2 (C sign, cubic HfO_2) nanoparticles.

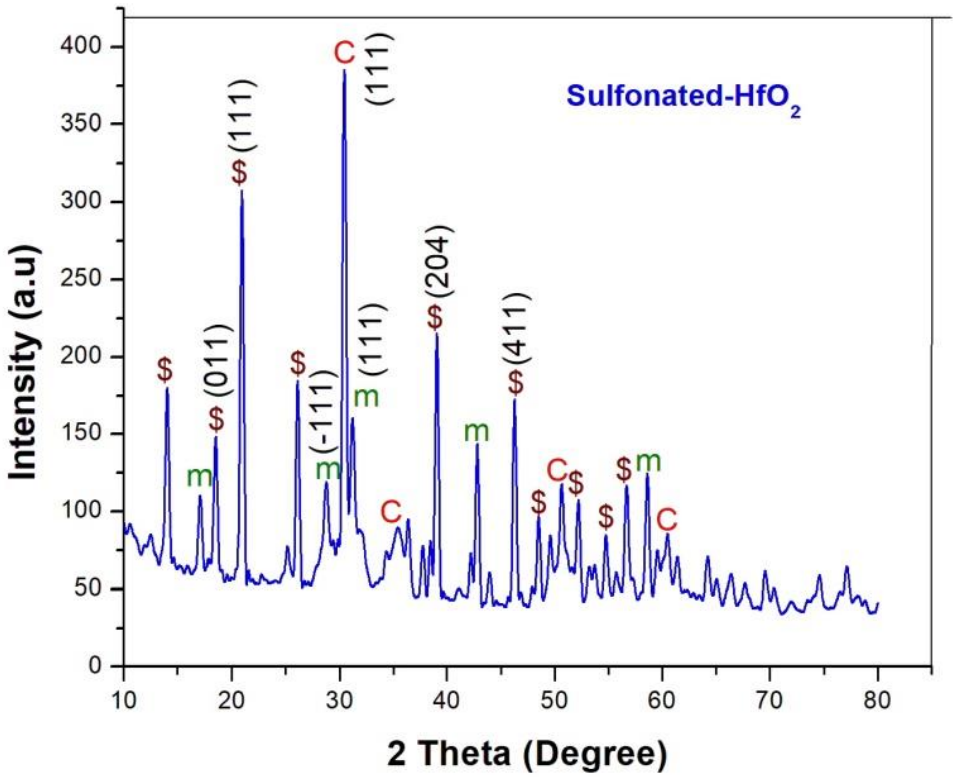

Fig. 2 XRD pattern S-HfO_2 (C, cubic HfO_2; m, monoclinic HfO_2; dollar sign, hafnium sulfate) nanoparticles.

Fig. 1 represents the XRD pattern of HfO_2 (before it was functionalized) nanoparticles which is exhibited in cubic phase. The main characteristic peaks at 24.23°, 30.47°, 35.41°, 50.79° and 60.20° on the 2θ scale were assigned to (110), (111), (200), (220) and (311) crystalline planes respectively, which is exactly in good agreement with the standard JCPDS card no. 53-0550 of cubic-HfO_2. **Fig. 2** represents the XRD pattern of S-HfO_2 (after functionalized) nanoparticles; which revealed that cubic and monoclinic phases of HfO_2 nanoparticles. The crystalline peaks at 24.23°, 30.47°, 35.41°, 50.79° and 60.20° were attributed to the cubic phase of HfO_2 planes (110), (111), (200), (220) and (311), respectively. But the peaks at 28.77° ($\bar{1}11$) and 31.41° (111) were assigned to the monoclinic crystalline planes of HfO_2. It is confirmed that

the monoclinic phase of HfO_2 were formed by influence of calcination (100°C for 24 h) during the sulfonation process. The crystallites size was calculated using a Debye Scherrer's formula [**23**]. The average crystallites size of the HfO_2 and S-HfO_2 nanoparticles were mentioned in Table 1. In addition to this, some peaks concur with the hafnium sulfate, such as 18.39°, 20.83°, 39.11° and 46.40° were assigned to (011), (111), (204) and (411) (JCPDS no. 24-0467) planes respectively. Hence, it was confirmed that oxidized sulfur groups, such as sulfones, sulfate or sulfonate were present in S-HfO_2.

3.2. Spectroscopic characterization of HfO_2 and S-HfO_2 nanoparticles

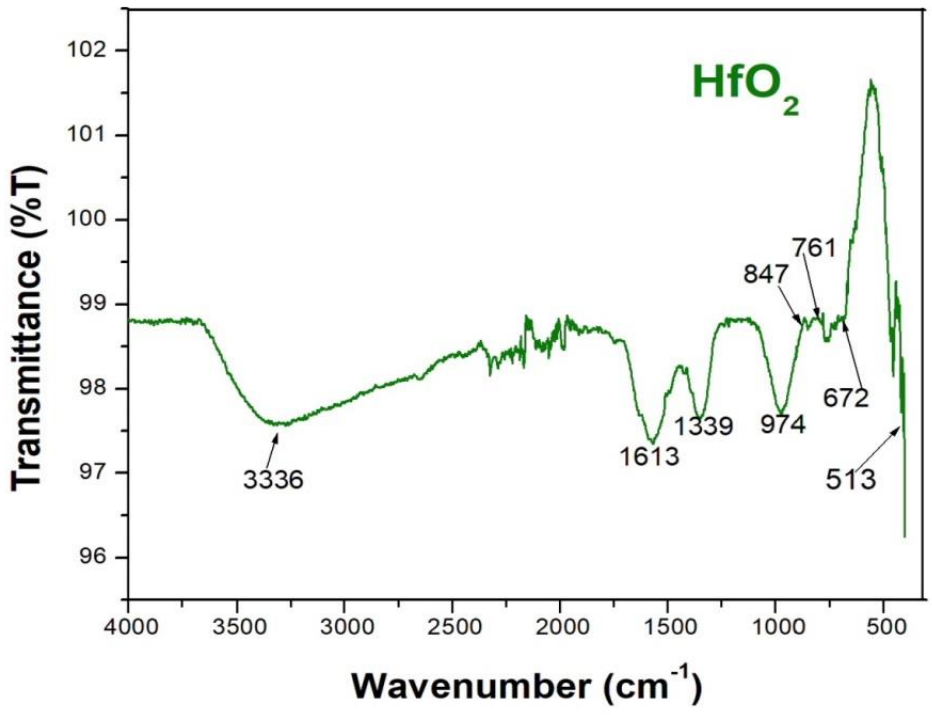

Fig. 3 FT-IR Spectrum of HfO_2 nanoparticles.

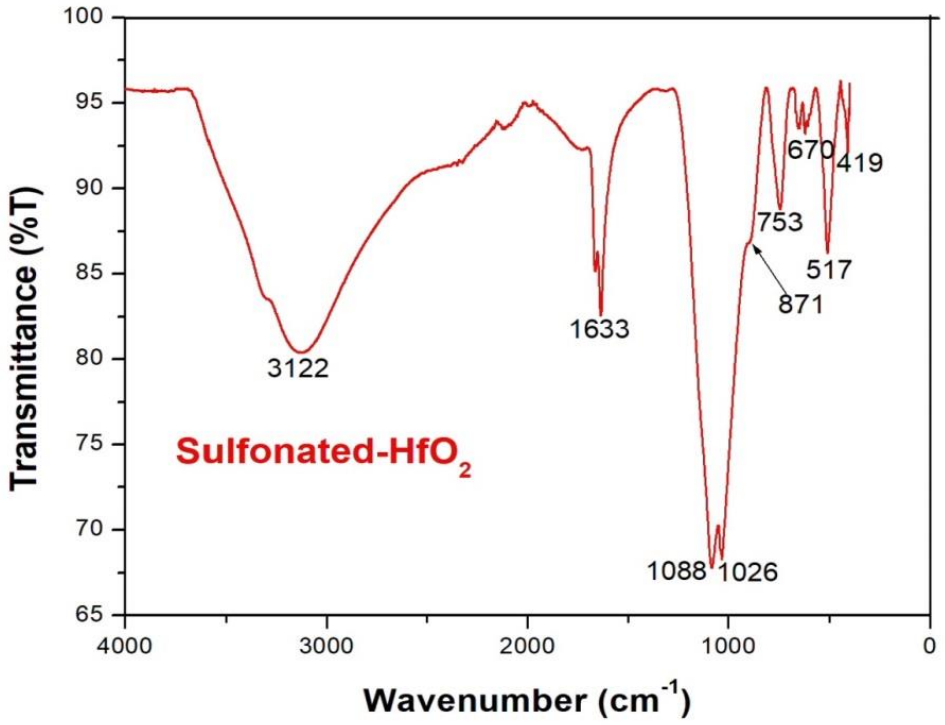

Fig. 4 FT-IR Spectrum of S-HfO_2 nanoparticles.

Fourier Transform Infrared (FTIR) spectroscopy has been performed for chemical identification of the prepared nanomaterial to find the presence of various bonds, and whether each bond vibrates at a specific frequency. The FT-IR spectra were taken in the ranges between 400 and 4000cm^{-1}. The characteristic peaks were observed at 761, 672 and 513 cm^{-1} in the **Fig. 4** were assigned to the Hf-O vibrational mode of HfO_2; Moreover, vibrational mode of HfO_2 is in the range of IR (800-400 cm^{-1}) active phonon modes of crystalline HfO_2 [19]. The position of these peaks is exactly coinciding with already reported theoretical values of monoclinic HfO_2 [**24**]. The absorption frequency found at 1613 cm^{-1} (**Fig. 3**) and 1633 cm^{-1} (**Fig. 4**) is assigned to the bending vibration of H-O-H bond and at 1339 cm^{-1} (**Fig. 3**) and is due to the bidentate carbonate symmetric stretching. These results were comparatively same as the already reported

literature results [**25**]. The absence of additional peaks in FT-IR spectra confirms the purity of the synthesized HfO_2 nanoparticles.

The **Fig. 4** represents the FT-IR spectra of functionalized hafnium oxide (S-HfO_2) nanoparticles. The peaks observed at 1088, 1026 and 871 cm^{-1} were due to the symmetric O=S=O, S=O and S-O stretching vibration of sulfonic acid group present in S-HfO_2 nanoparticles respectively. In addition to this the broad peak found at 3122 cm^{-1} is due to the –OH (water molecules) stretching vibration and is absorbed by the sulfonic (-SO_3H) group [**26-29**].

3.2 Surface Morphology of HfO_2 (before it was functionalized) and S-HfO_2 (after it was functionalized)

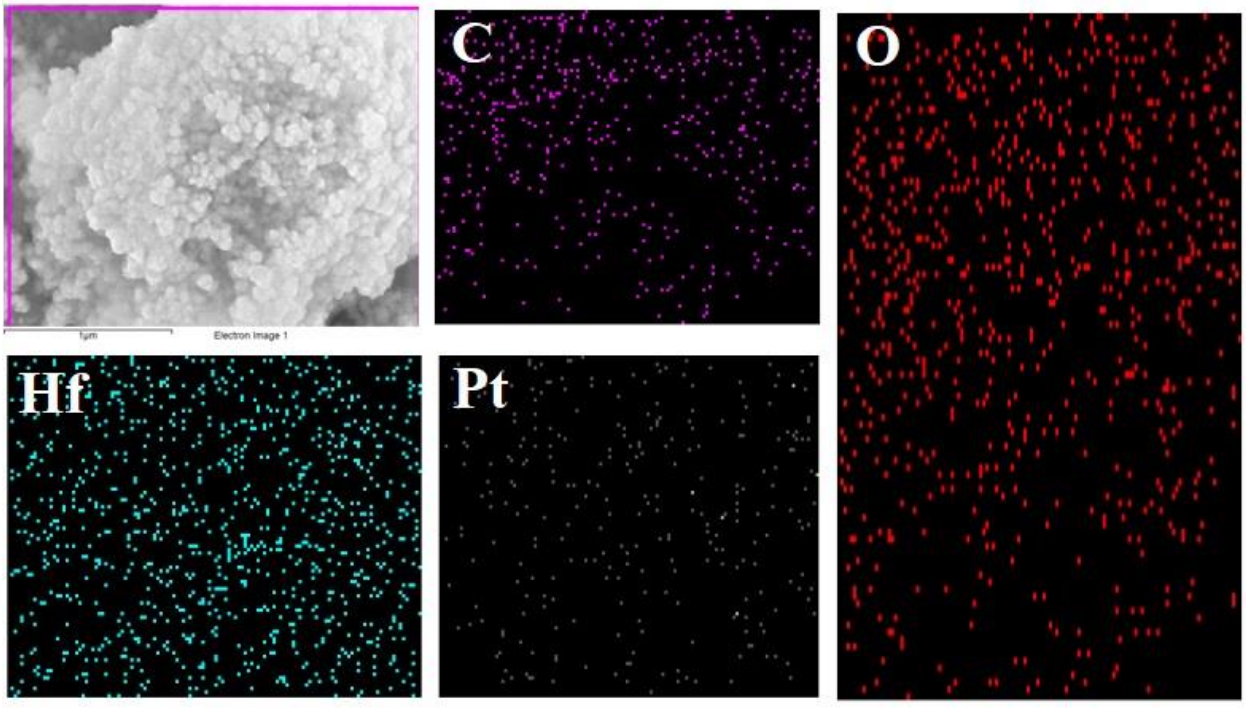

Fig. 5 Mapping of SEM with EDS of HfO_2 (before it was functionalized) nanoparticles.

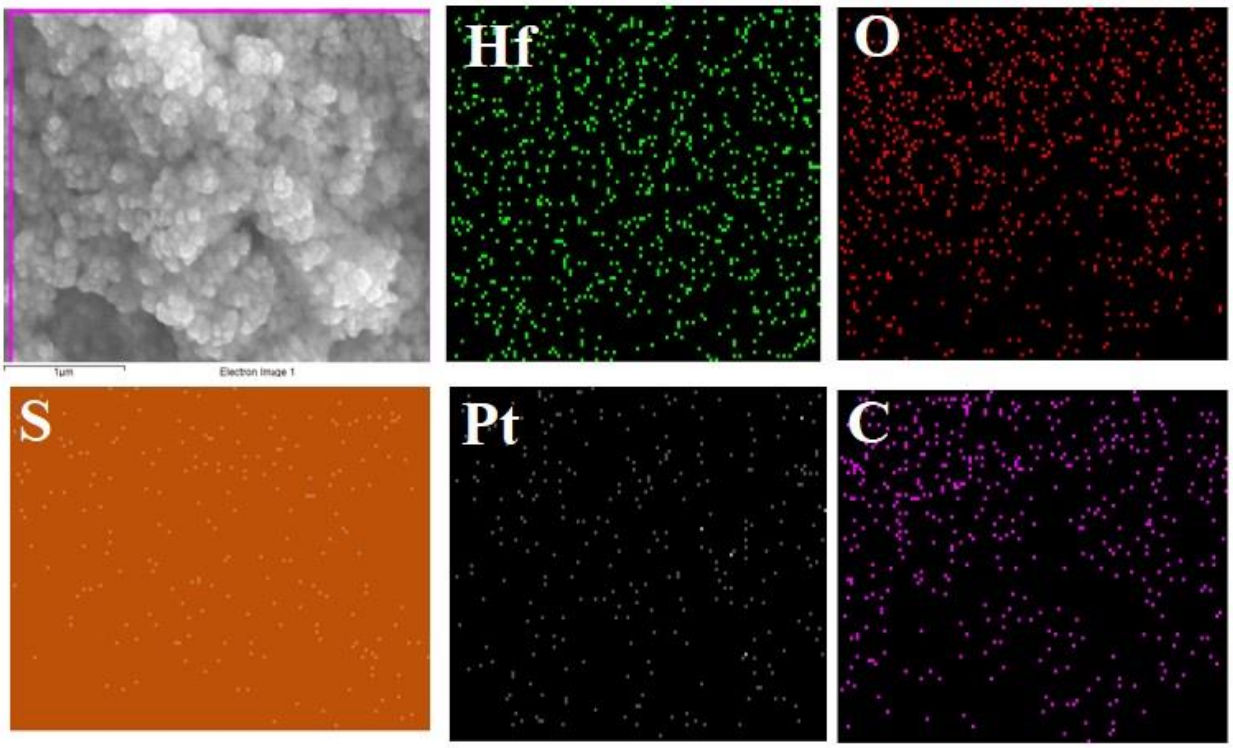

Fig. 6 Mapping of SEM with EDS of S-HfO_2 (after it was functionalized) nanoparticles

SEM – EDS analysis was performed to determine the surface morphology of HfO_2 (before it was functionalised) nanoparticles. **Fig.5** shows the SEM-EDS mapping image of HfO_2 nanoparticles, which reveal the presence carbon (C), oxygen (O), hafnium (Hf) and platinum (Pt) present in the HfO_2 nanoparticles. Moreover, from the **Fig. 5** we observed that the HfO_2 particles were fine microstructure and uniform distribution of dense particles, spherical shaped and agglomerated with each other [**30**]. The average grain sizes observed from SEM image were found to coincide well with the calculated grain size using XRD data. In addition to this, SEM-EDS was performed to S-HfO_2 (after functionalised) nanoparticles, which was used to examine the dispersion and presence of sulfonic group in HfO_2 nanoparticles. Moreover, the presence of additional image (S) in **Fig. 6** was attributed to sulfonic groups that were functionalised

uniformly with HfO_2 particles. Consequently it also confirmed that ($-SO_3H$) group is more compatible with HfO_2 nanoparticles.

Furthermore, the elements present on the surface of the S-HfO_2 nanoparticles were identified using EDS analysis as is shown in the **Fig. 5** (a, HfO_2) and (b, S-HfO_2) respectively. It was observed that, the sulfur (S) element was present on the surface of the HfO_2 nanoparticles, which revealed that, the organic grafted sulfonic acid group ($-SO_3H$) had condensed with the hydroxyl groups of HfO_2 [**31,32**].

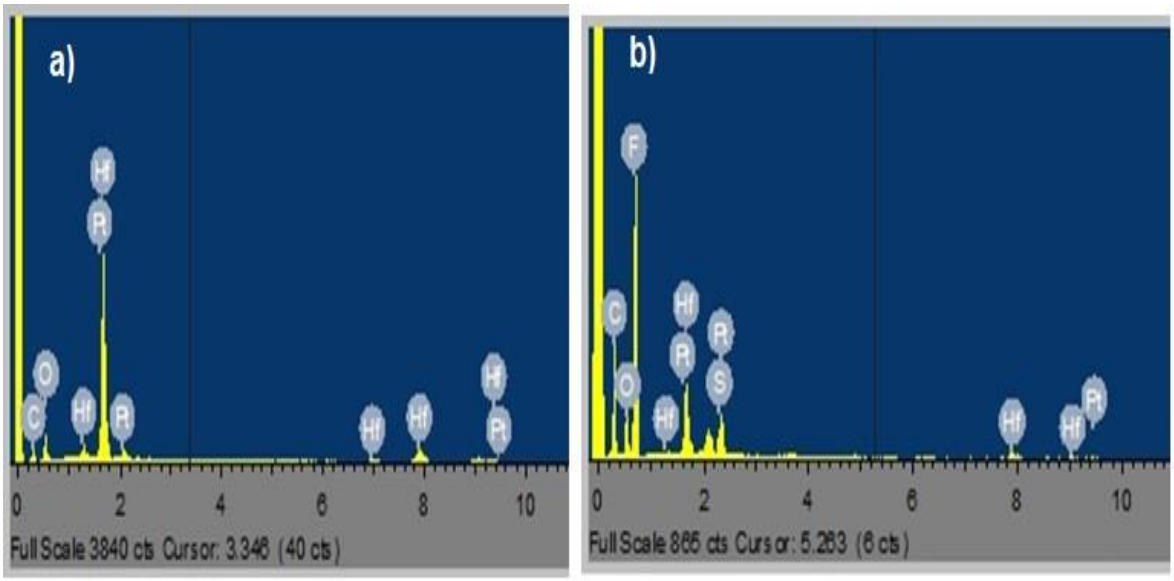

Fig. 7 EDS Analysis results of HfO_2 (a) and S-HfO_2 (b) Nanoparticles.

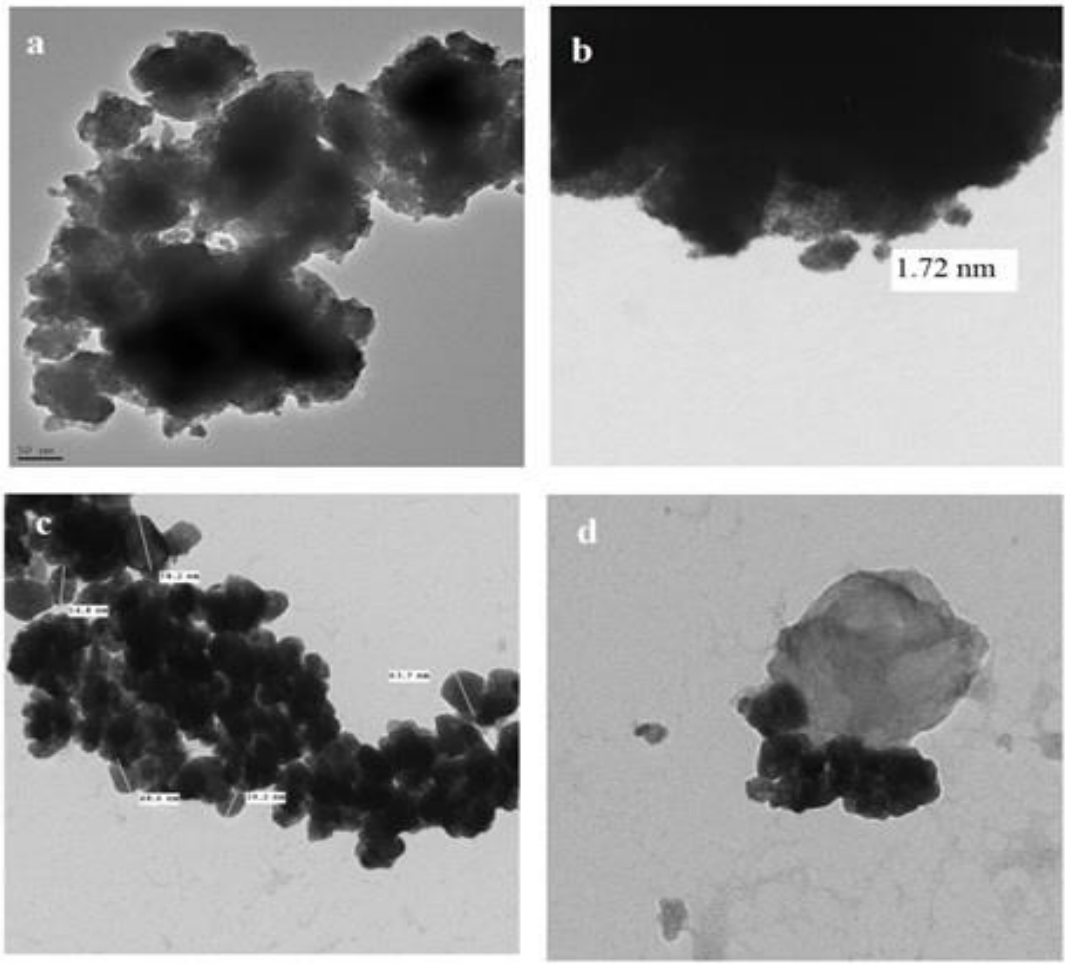

Fig. 8 HR-TEM images of HfO_2 (a & b) and S-HfO_2 (c & d) nanoparticles.

The surface morphology of HfO_2 and changes in surface morphology of S-HfO_2 (after it was functionalised) were also observed by HRTEM which is showed in **Fig. 8** It is clear that all the HfO_2 NPs aggregated and were amorphous, spherical like / interconnected with each other due to high stressed and temperature diffusion [**33**]. The particle size is ranged from 10 to 70 nm (**Fig. 8a**). The S-HfO_2 nanoparticles in **Fig. 8 (c & d)** showed spherical bud shaped and aggregated with other particles. Consequently, the spherical size of S-HfO_2 were futher reduced **(Fig. 8(c))** may due to under sulfonation process of HfO_2 nanoparticles.

3.3. Electrochemical behavior of HfO_2 and S-HfO_2 nanoparticles

To identify the usefulness of functionalized HfO_2 (S-HfO_2) nanoparticles as electrode materials, their electrochemical properties were assessed. So the pseudo-capacitance of HfO_2 and functionalized S-HfO_2 nanoparticles has been evaluated by cyclic voltammetry method. CV studies were recorded by the three traditional electrode system [**34**] composed of HfO_2 and/or S-HfO_2 (working electrode), standard calomel electrode (counter electrode) and platinum wire (reference electrode) in 1.0 M H_2SO_4 electrolytes; applied potential ranges from 0 to 0.8V with sweep rates (5 to 50 mVs^{-1}). **Fig. 9** shows cyclic voltammograms of HfO_2 and S-HfO_2.

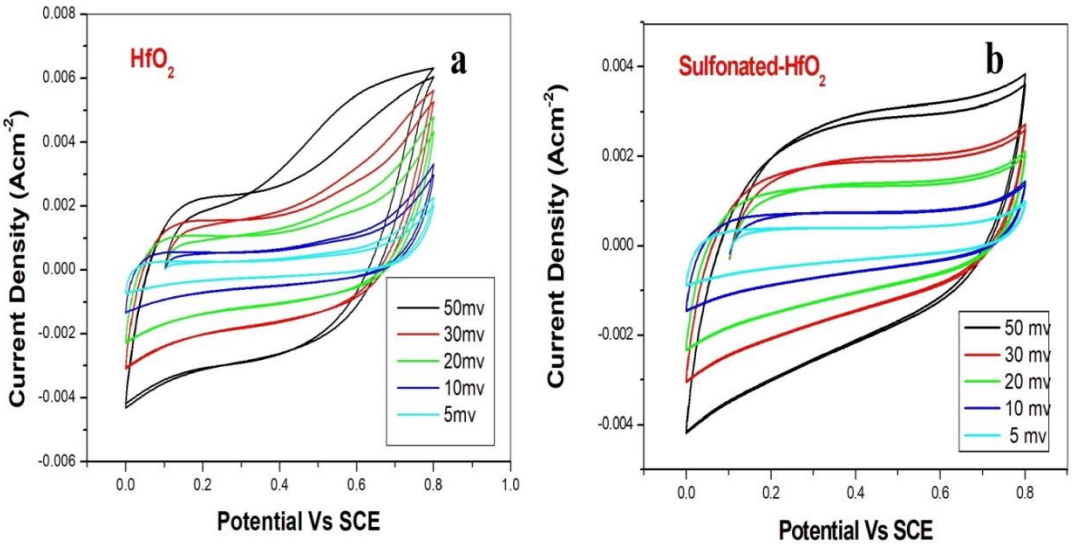

Fig. 9 Cyclic voltammetry curves of HfO_2 (a) and functionalized S-HfO_2 (b) electrode at different scan rates in 1M H_2SO_4 electrolyte.

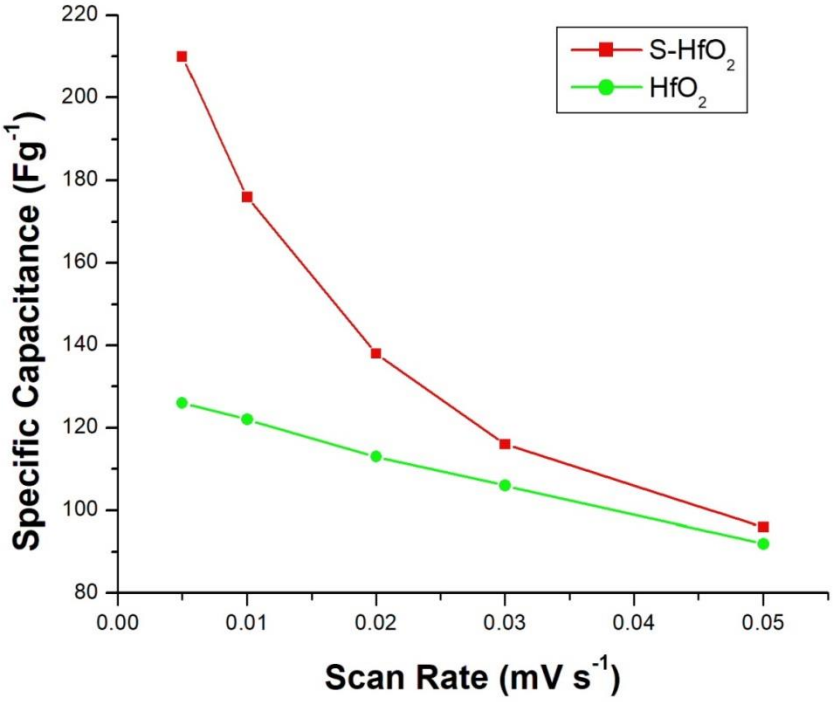

Fig. 10. Variation of specific capacitance of HfO_2 and S-HfO_2 electrodes with scan rate.

There was a characteristic difference of the electrochemical activity in **Fig. 9** between glassy carbon electrodes coating with and without of HfO_2/S-HfO_2 nanoparticles. The characteristic redox peaks in the CV curve of S-HfO_2 shows in **Fig. 9b** reveals that current density is increased while the scan rate is increased gradually. This behavior in the CV is due to the transport of ions onto the surface of the electrode through $–SO_3H$ groups in S-HfO_2 [**35**]. Obviously, the specific capacitance has been increased by decreasing the scan rate which is present in **Fig. 10** In addition to this, CV curve area of S-HfO_2 is larger than that of HfO_2 which illustrates that the electrochemical performance of S-HfO_2 nanoparticles is highly improved owing to the presence of sulfonic group. However, the peak current density almost linearly depends on the scan rate, which reveals a controlled redox process and the excellent rate

capability of the S-HfO_2 electrode. The electrochemical behavior of the S-HfO_2 electrode material demonstrates that the functionalized S-HfO_2 nanoparticle is equipped with excellent electrochemical properties [**36**].

Table-1: Specific capacitance values of HfO_2 and S-HfO_2 from CV and GCD techniques

S. No.	Specific Capacitance (F/g) in 1M H_2SO_4										
	Product	Size (nm)	CV Voltage Scan Rate (mVs^{-1})					Galvanostatic Charge/Discharge (GCD) Current Density (Ag^{-1})				
			5	10	20	30	50	0.2	0.3	0.4	0.5	1
1.	HfO_2	10-70	126	122	113	106	92	107.63	81.25	53.25	38.56	13.25
2.	S-HfO_2	20-60	210	176	138	116	96	200.63	110.94	76.43	65.23	38.63

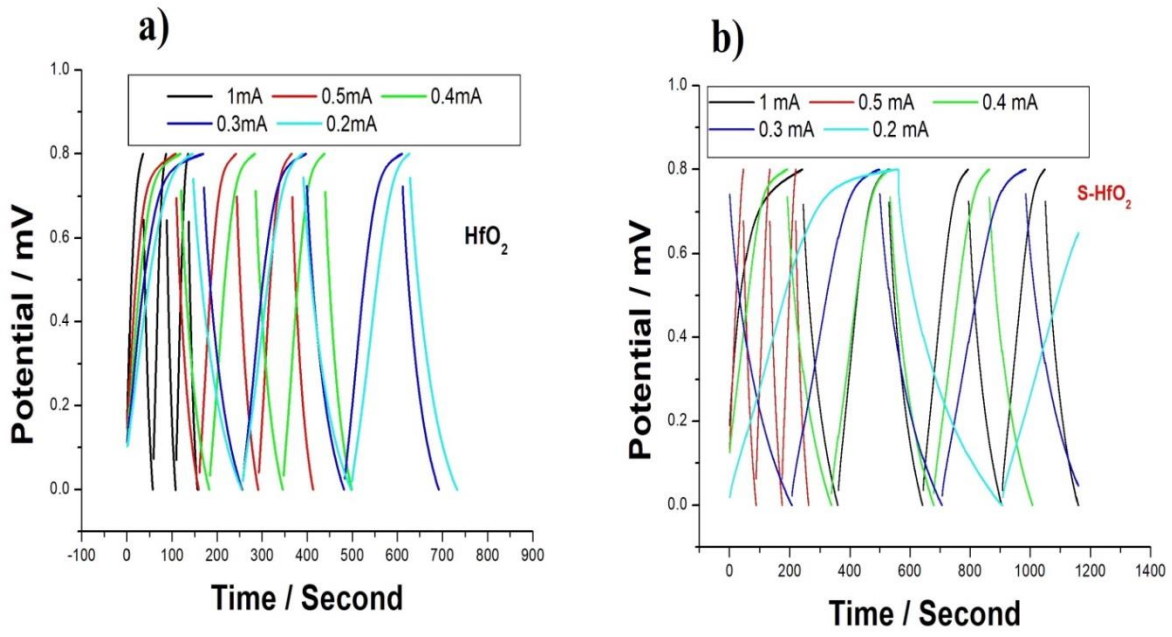

Fig. 11 Charge/Discharge curves of HfO_2 and S-HfO_2 nanoparticles.

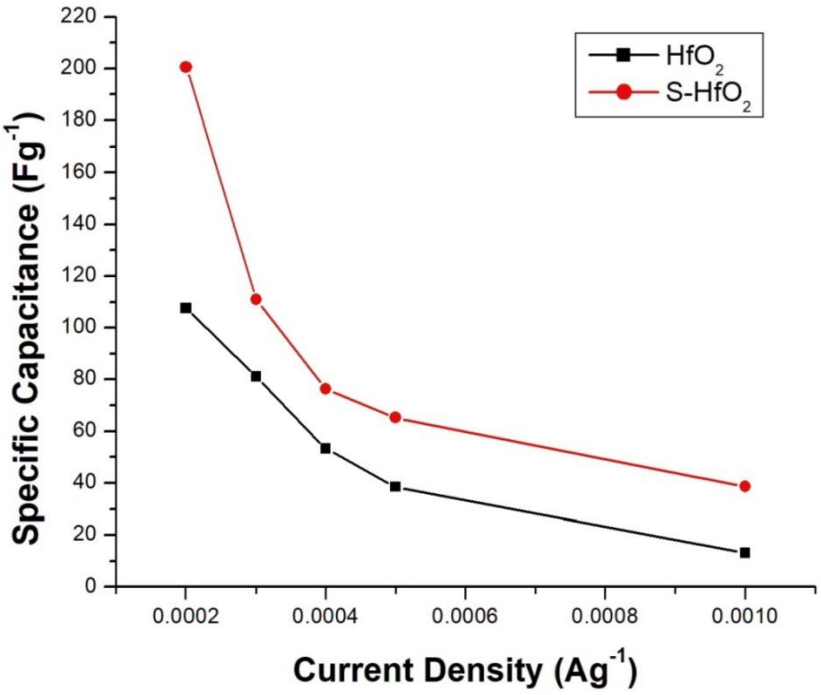

Fig. 12. Variation of specific capacitance of HfO_2 and S-HfO_2 electrodes with current density.

Cycle stability is one of the most important criteria for supercapacitor applications. In order to find out the cycle stability of HfO_2 and S-HfO_2 nanoparticle electrodes in 1.0 M aq. H_2SO_4 electrolyte was evaluated by galvanostatic charge-discharge measurement ranges from 0.2 Ag^{-1} to 1 Ag^{-1} and the potential ranges between 0 and 0.8 V. All the charge/discharge curves of the HfO_2 and S-HfO_2 nanoparticles displayed nearly symmetric and equivalent triangular shapes (**Fig. 11**). It was a good evidence of excellent capacitance. These charge/discharge curves further indicated a good reversibility in the course of the charge/discharge process. The discharge curves of S-HfO_2 showed an evident pseudo-capacitance performance as they deviated from a perfect linear shape. Moreover, the redox peaks of S-HfO_2 were present in positive potential is

influenced by the presence of $–SO_3H$ that increases the conductivity of the nanoparticles, thereby facilitating the charge transfer mechanism. The specific capacitances of the HfO_2 and S-HfO_2 were calculated using the various sweep rates (i.e. 0.2 mA, 0.3mA, 0.4mA, 0.5mA and 1mA) and their values are tabulated in Table (1). For HfO_2 the specific capacitance value ranges from 13.25 Fg^{-1} to 107.63 Fg^{-1} but S-HfO_2 has increased ranges between 38.63 Fg^{-1} and 200.63 Fg^{-1}. The higher capacitance of S-HfO_2 is due to increased surface area and an additional pseudo-capacitance owing to the presence of oxygen-containing functional groups ($–SO_3H$) in HfO_2 nanoparticles [**37-40**]. The specific capacitance (200.63 Fg^{-1}) value of S-HfO_2 is comparably high with HfO_2.

Moreover, the specific capacitance increases while decreasing the current density as is displayed in **Fig. 12** The specific capacitances under constant current in three electrode system (GCD) were calculated according to this (C_{sp} (F/g) = $I\Delta t/\Delta Em$) equation.

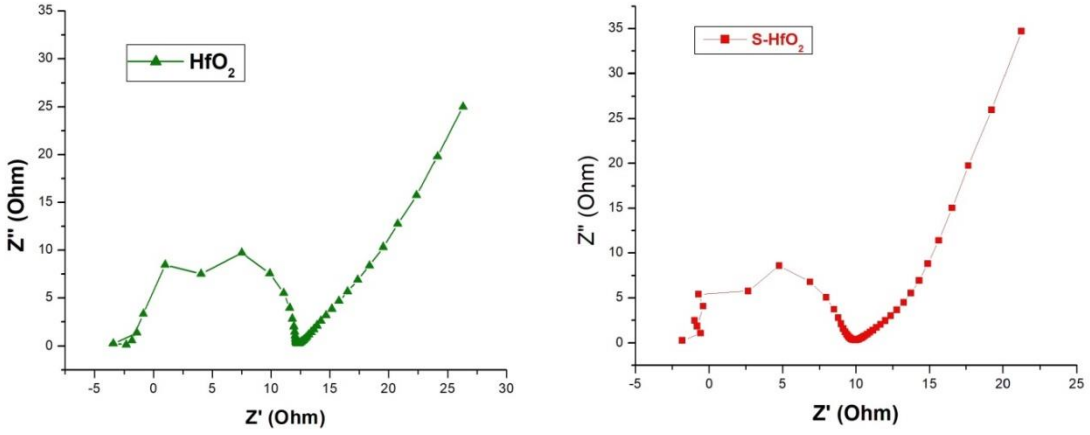

Fig. 13 Nyquist Impedance plots of HfO_2 and S-HfO_2 electrodes.

To understand more about supercapacitive performance, the internal resistance of electrodes were analysed using EIS technique. **Figure 13** shows the EIS data were analysed by the Nyquist plot of the prepared electrode (HfO_2 and S-HfO_2). In a Nyquist plot the imaginary component (Z″) of the impedance plotted versus the real component (Z′). The Nyquist plots of the two samples (HfO_2 and S-HfO_2) consist of an incomplete semicircle at high frequency and a slope line (Warburg region) at low frequency, this indicating that the electrode process is in the control of both charge transfer and diffusion processes. The interfacial charge transfer resistance (R_{ct}) between electrode and electrolyte is responsible for the generation of the incomplete semicircle [**41**]. The supercapacitor behaviour of an electrode increases with increasing the slope of the vertical line. Moreover, the reason for the generation of a Warburg region is that the charge transfer rate is larger than the ion-diffusion rate. The major difference is that the HfO_2 showed a slightly larger semicircle than the S-HfO_2 nanoparticles in the intermediary frequency range, indicating a higher charge transfer resistance because HfO_2 is a semiconductor and the conductivity of S-HfO_2 nanoparticles increased due to the $–SO_3H$ group on the surface of the HfO_2. Another difference is the straight line inclined at an angle of around 45° to the real axis (Z') in the intermediate-frequency region, corresponding to the semi-infinite ion diffusion resistance; compared to HfO_2, the process of S- HfO_2 nanoparticles electrodes is under the control of diffusion in the lower-frequency. At high frequency, the behaviour of the supercapacitor is mainly resistive. As shown in **Fig. 13** the differences between the Nyquist plots of the HfO_2 and S-HfO_2 nanoparticles reflected due to the functional group ($–SO_3H$), changing the conductivity and the properties of the electrode/electrolyte interface [**42**]. On the other hand, the long-term electrochemical stability of the prepared materials is attributed to the presence of a

$-SO_3H$ functional group on HfO_2 nanoparticles. The hydrophilic nature of $-SO_3H$ increases the wettability of the electrode and thus enhances the SC performance [**43**].

4. Conclusions

HfO_2 nanoparticle was synthesized by a precipitation method and it was functionalized using sulphuric acid. The HfO_2 and functionalized HfO_2 (S-HfO_2) nanoparticles were characterized by XRD, FT-IR, FE-SEM, EDS and HR-TEM. Further, the supercapacitance performance of both intrinsic HfO_2 and S-HfO_2 were evaluated using cyclic voltammetry technique and it was found to be 210 Fg^{-1} for S-HfO_2 and for intrinsic HfO_2 was 126 Fg^{-1}. It was found that the S-HfO_2 nanoparticles having superior SC than intrinsic HfO_2 and S-HfO_2 can be a promising candidate for energy applications. Importantly, electrochemical impedance spectroscopies demonstrate that -SO_3H group not only provide the electron transfer channels for HfO_2, but also benefit the electrolyte penetration in HfO_2 nanomaterials.

References

1. M. Nakamura, M. Nakanishi, K. Yamamoto, Influence of Physical Properties of Activated Carbons on Characteristics of Electric Double-Layer Capacitors, J. Power Sources, **60**, 225-231 (1996)
2. M. Winter, R.J. Brodd, What Are Batteries, Fuel Cells and Supercapacitors?, Chem. Rev., **104**, 4245-4268 (2004)
3. C. Du, N. Pan, High power density dupercapacitor electrodes of carbon nanotube films by electrophoretic deposition, Nanotech., **17**, 5314-5318 (2006)
4. C. Bora, J. Sharma, S. Dolui, Polypyrrole/Sulfonated Graphene Composite as Electrode Material for Supercapacitor, J. Physical Chem. C, **118**, 29688-29694 (2014)
5. X. Sun, M. Xie, G. Wang, H. Sun, A.S. Cavanagh, J.J. Travis, S.M. George, J. Liana, Atomic Layer Deposition of TiO_2 on Graphene for Supercapacitors, J. Electrochem. Soc., **159**, A364-A369 (2012)
6. K. Naoi, P. Simon, New Materials and New Configurations for Advanced Electrochemical Capacitors, Electrochem. Soc. Interface, **17**, 34-37 (2008)
7. J. Jiang, A. Kucernak, Electrochemical supercapacitor material based on manganese oxide: preparation and characterization, Electrochim. Acta, **47**, 2381-2386 (2002)
8. Y.Y. Xi, D. Li, A.B. Djurisic, M.H. Xie, K.Y.K. Man, W.K. Chan, Hydrothermal Synthesis vs Electrodeposition for High Specific Capacitance Nanostructured NiO Films, Electrochem. and Solid-State Letters, **11**, D56-D59 (2008)
9. T.C. Liu, W.G. Pell, B.E. Conway, Stages in the development of thick cobalt oxide films exhibiting reversible redox behavior and pseudocapacitance, Electrochim. Acta, **44**, 2829-2842 (1999)

10. V. Srinivasan, J.W. Weidner, Capacitance studies of cobalt oxide films formed via electrochemical precipitation, J. Power Sources, **108**, 15-20 (2002)
11. T. Brousse, D. Belanger, A Hybrid Fe_3O_4 - MnO_2 Capacitor in Mild Aqueous Electrolyte, Electrochem. and Solid-State Letters, **6**, A244 (2003)
12. N.L. Wu, S.Y. Wang, C.Y. Han, D.S. Wu, L.R. Shiue, Electrochemical capacitor of magnetite in aqueous electrolytes, J. Power Sources, **113**, 173-178 (2003)
13. H., Mudila, S. Rana, M.G.H. Zaidi, Electrochemical performance of zirconia/graphene oxide nanocomposites cathode designed for high power density supercapacitor, J. Analytical Sci. and Technol., **7**, 1-11 (2016)
14. H. Huang, W.K. Zhang, X.P. Gan, C. Wang, L. Zhang, Electrochemical investigation of TiO_2/carbon nanotubes nanocomposite as anode materials for lithium-ion batteries, Materials Lett., **61**, 296-299 (2007)
15. J. Venkatachalam, B. Ganesan, C. Shanmugavel, G. Singaravelu, A. Prakasarao, Synthesis and characterization of hafnium oxide nanoparticles for bio-safety, Materials Exp., **4**, 375-383 (2014)
16. M. Jayavel, N. Ramalakshmi, S. Arul Antony, J. Venkatachalam, Hafnium Oxide/Graphene Oxide Nanocomposites as Efficient Supercapacitor Electrodes, J Nanosci. and Technol., **4**, 383-387 (2018)
17. P. Bandyopadhyay, T. Kuila, J. Balamurugan, T.T. Nguyen, N.H. Kim, J.H. Lee, Facile synthesis of novel sulfonated polyaniline functionalized graphene using m-aminobenzene sulfonic acid for asymmetric supercapacitor application, Chem. Engg. J., **308**, 1174-1184 (2017)

18. S.S. Karade, S.S. Raut, H.B. Gajare, B.R. Nikam, R. Sharma, B.R. Sankapal, Widening potential window of flexible solid-state supercapacitor through asymmetric configured iron oxide and poly(3,4-ethylenedioxythiophene) polystyrene sulfonate coated multi-walled carbon nanotubes assembly, J. Energy Storage, **31**, 101622 (2020)
19. A. Ramadoss, K. Krishnamoorthy, S.J. Kim, Novel synthesis of hafnium oxide nanoparticles by precipitation method and its characterization. Materials Research Bulletin, **47**, 2680-2684 (2012)
20. S. Ayyaru, Y.H. Ahn, Application of sulfonic acid group functionalized graphene oxide to improve hydrophilicity, permeability, and antifouling of PVDF nanocomposite ultrafiltration membranes, J. Membr. Sci., **525**, 210-219 (2017)
21. S. Ayyaru, Y.H. Ahn, Fabrication and separation performance of polyethersulfone/sulfonated TiO_2 (PES–$STiO_2$) ultrafiltration membranes for fouling mitigation, J. Industrial and Engg. Chem., **67**, 199-209 (2018)
22. P. Sivakumar, R. Ramesh, P. Ramanand, Ponnusamy, S., C. Muthamizhchelvan, Synthesis and characterization of nickel ferrite magnetic nanoparticles, Materials Research Bulletin, **46**, 2208-2211 (2011)
23. T. Kidchob, L. Malfatti, F. Serra, P. Falcaro, S. Enzo, P. Innocenzi, Hafnia sol-gel films synthesized from HfCl4: Changes of structure and properties with the firing temperature, J. Sol-Gel Sci. and Technol., **42**, 89-93 (2007)
24. D.A. Neumayer, E. Cartier, Materials characterization of ZrO_2–SiO_2 and HfO_2–SiO_2 binary oxides deposited by chemical solution deposition, J. Appl. Phy., **90**, 1801-1808 (2001)

25. A. Sivasankaran, D. Sangeetha, Influence of sulfonated SiO_2 in sulfonated polyether ether ketone nanocomposite membrane in microbial fuel cell. Fuel, **159**, 689-696 (2015)
26. N. Kumar, B.P.A. George, H. Abrahamse, V. Parashar, S.S. Ray, J.C. Ngila, A Novel approach to low temperature synthesis of cubic HfO_2 nanostructures and their cytotoxicity, Scientific Reports, **7**,1-14 (2017)
27. A. Ramadoss, S.J. Kim, Synthesis and characterization of HfO_2 nanoparticles by sonochemical approach, J. Alloys and Compds., **544**, 115-119 (2012)
28. D. Zhao, B.L. Yi, H.M. Zhang, H.M. Yu, $MnO_2/SiO_2–SO_3H$ nanocomposite as hydrogen peroxide scavenger for durability improvement in proton exchange membranes, J. Member Sci., **346**, 143-151 (2010)
29. V. Balan, C.T. Mihai, F.D. Cojocaru, C.M. Uritu, G. Dodi, D. Botezat, I. Gardikiotis, Vibrational Spectroscopy Fingerprinting in Medicine: from Molecular to Clinical Practice, Materials, **12**, 01-40 (**2019**)
30. M. Jayavel, N. Ramalakshmi, S. Arul Antony, Synthesis, Characterization and Cytocompatibility of HfO_2 Nanoparticle Against A549 Cell Lines with Potent Antimicrobial Activities, J. Nanosci. and Technol., **3**, 245-248 (2017)
31. S. Ayyaru, S. Dharmalingam, Improved performance of microbial fuel cells using sulfonated polyether ether ketone (SPEEK) $TiO_2–SO_3H$ nanocomposite membrane, RSC Advances, **3**, 25243-25251 (2013)
32. S. Ayyaru, Y.H. Ahn, Fabrication of a Novel Nanocomposite Ultrafiltration Membrane with Improved Antifouling Properties Using Functionalized HfO_2 and Polyvinylidene Fluoride for Organic Foulant Mitigation, Indust. & Engg. Chemistry Res., **59**, 19272-19284 (2020)

33. C.V. Ramana, K. Kamala Bharathi, A. Garcia, A.L. Campbell, Growth Behavior, Lattice Expansion, Strain, and Surface Morphologyof Nanocrystalline, Monoclinic HfO_2 Thin Films, J. Phys. Chemistry C, **116**, 9955-9960 (2012)
34. S.A. El-Khodary, G.M. El-Enany, M. El-Okr, M. Ibrahim, Modified iron doped polyaniline/sulfonated carbon nanotubes for all symmetric solid-state supercapacitor, Syn. Metals, **233**, 41-51 (2017)
35. E. Cevik, S.T. Gunday, A. Yusuf, M.A. Almessiere, A. Bozkurt, Boron-incorporated Sulfonated polysulfone/polyphosphoric acid electrolytes for supercapacitor application, Soft Materials, **17**, 203-211 (2019)
36. H.B. Zhao, J. Yang, T.T. Lin, Q.F. Lu, G. Chen, Nanocomposites of Sulfonic Polyaniline Nanoarrays on Graphene Nanosheets with an Improved Supercapacitor Performance, Chemistry A European J., **21**, 682-690 (2014)
37. J. Zhang, X.S. Zhao, Conducting Polymers Directly Coated on Reduced Graphene Oxide Sheets as High-Performance Supercapacitor Electrodes, J. Physical Chemistry C, **116**, 5420−5426 (2012)
38. Z. Xiong, T. Gu, X. Wang, Self-Assembled Multilayer Films of Sulfonated Graphene and Polystyrene-Based Diazonium Salt as Photo-Cross-Linkable Supercapacitor Electrodes, Langmuir, **30**, 522-532 (2014)
39. X. Zuo, Y. Zhang, L. Si, B. Zhou, B. Zhao, L. Zhu, X. Jiang, One-step electrochemical preparation of sulfonated graphene/polypyrrole composite and its application to supercapacitor, J. Alloys and Compds., **688**, 140-148 (2016)

40. Q. Wang, N. Plylahan, M.V. Shelke, R.R. Devarapalli, M. Li, P. Subramanian, T. Djenizian, R. Boukherroub, S. Szunerits, Nanodiamond particles/reduced graphene oxide composites as efficient supercapacitor electrodes, Carbon, **68**, 175-184 (2014)
41. B.Y. Chang, S.M. Park, Integrated Description of Electrode/Electrolyte Interfaces Based on Equivalent Circuits and Its Verification Using Impedance Measurements, Analytical Chemistry, **78**, 1052-1060 (2006)
42. L. Lu, Y. Zhu, F. Li, W. Zhuang, K.Y. Chan, X. Lu, Carbon titania mesoporous composite whisker as stable supercapacitor electrode material, J. Materials Chemistry, **20**, 7645-7651 (2010)
43. T. Kuila, A.K. Mishra, P. Khanra, N.M. Kim, M.E. Uddin, J.H. Lee, Facile Method for the Preparation of Water Dispersible Graphene using Sulfonated Poly(ether−ether−ketone) and Its Application as Energy Storage Materials, Langmuir, **28**, 9825-9833 (2012)